

# Robust Beamforming Algorithms for Acoustic Tracking of Ground Vehicles

Nicholas J. Roseveare<sup>a</sup> and Mahmood R. Azimi-Sadjadi<sup>b</sup>

<sup>a</sup> Department of Electrical and Computer Engineering, Colorado State University, Fort Collins, CO, 80523 USA;

<sup>b</sup>Information System Technologies, Inc., 425 Mulberry West, Suite 108, Fort Collins, CO, 80521 USA

## ABSTRACT

The problem of detection and localization of multiple acoustic sources using unattended passive sensors is considered. Existing wideband Capon direction of arrival (DOA) estimation methods typically fail to accurately detect and resolve multiple closely spaced sources in presence of model mismatches and wavefront perturbations caused by sensor location errors and near-field effects. This paper applies a set of adaptive beamforming methods in reduced dimension subspace for non-ideal acoustic array sensing scenarios. A robust wideband Capon method is studied to account for the inherent uncertainties in the array steering vector. To improve the resolution within a sector of interest the beamspace method is extended and applied to this problem. These methods are then implemented and benchmarked on real acoustic signatures of multiple ground vehicles moving in tight formations.

**Keywords:** Unattended Acoustic Sensors, Robust Beamforming, Sensor Location Error

## 1. INTRODUCTION

Unattended passive acoustic sensors are becoming increasingly popular for a variety of military applications including remote battlefield surveillance, situation awareness and monitoring.<sup>1-3</sup> They are rugged, reliable, and can be left in the field for a relatively long period of time after deployment. They can be used to capture acoustic signatures of a wide variety of targets including ground targets, airborne targets, gunshots, or personnel. The signatures of these sources typically overlap both temporally and spectrally. Clearly, in these applications optimum sensor performance for detection, tracking, and classification of multiple sources is highly dependent on terrain, weather, and background noise.

The problem of detection, classification and localization of multiple ground targets, e.g. trucks and tanks, using unattended passive acoustic sensors is complicated due to various factors. These include: variability and nonstationarity of source acoustic signatures, signal attenuation and fading effects as a function of range and doppler, coherence loss due to environmental conditions and wind effects, near field and non-plane wave effects, and high levels of acoustic clutter and interference. In addition, presence of multiple closely spaced targets that move in tight formations, e.g. staggered, abreast or single-file, further complicates the direction of arrival (DOA) estimation and localization processes.

Previous work involved development of wideband array processing algorithms for baseline acoustic circular arrays to detect and track moving targets from their acoustic signatures.<sup>1-3</sup> Current efforts<sup>4</sup> on incoherent and coherent wideband MUSIC<sup>5</sup> (Multiple Signal Classification) show some promise for detecting and tracking multiple ground vehicles. Recently, by exploiting the multi-spectral content of the targets, better results were reported using wideband signal subspace DOA algorithms.<sup>2</sup> Experimental results using a circular array of six sensors, with a diameter of 8 ft indicated the advantages of the wideband MUSIC over the delay-sum algorithm. In<sup>3</sup>, focused wideband adaptive array processing algorithms are employed for the high-resolution DOA estimation

---

Further author information: (Send correspondence to M.R. Azimi-Sadjadi)  
M.R. Azimi-Sadjadi: E-mail: mo@infsyst.biz, Telephone: 1 970 491 7956  
N.J. Roseveare: E-mail: nrosev@engr.colostate.edu, Telephone: 1 970 491 1518

of ground vehicles. Several methods including Steered Covariance Matrix (STCM)<sup>4-7</sup> and spatial smoothing using the array manifold interpolation<sup>4</sup> were considered. In addition, experimental analysis of DOA accuracy of incoherent and coherent wideband MUSIC algorithms and narrowband MUSIC for a circular array of acoustic sensors was provided. It was shown that in certain SNR conditions incoherent wideband methods yield more accurate DOA estimates than the coherent methods especially for highly peaked spectra, such as those of typical machinery, while for sources with flat spectra the coherent wideband methods generate more accurate DOA estimates. Three new wideband DOA estimation methods were recently developed<sup>8</sup> to resolve the issues with the focusing process in other wideband algorithms (such as the STCM algorithm<sup>9</sup>) and also to improve the accuracy of DOA estimation. These algorithms are based upon wideband extension of the Capon beamforming.<sup>5</sup> Three different methods for combining individual narrowband Capon power spectra at different frequency bins were introduced based upon arithmetic mean, geometric mean, and harmonic mean operations.<sup>8</sup> The beampatterns and bearing responses of these wideband Capon beamformers at various frequencies were also studied in order to evaluate their ability to resolve multiple closely spaced sources.

However, the existing algorithms lack the proven capability to detect and track multiple closely spaced sources in tight formations especially in the presence of array manifold mismatches, wavefront perturbations and near-field effects. This is critical in realistic battlefield scenarios owing to the variability in the environmental and operating conditions, and uncertainty in sensor locations.

To overcome these problems and improve robustness of current wideband DOA estimation methods<sup>8</sup> the robust Capon beamforming method<sup>10</sup> is extended in this paper. This particular method provides robustness to array manifold mismatches and wavefront perturbations and hence helps to decrease tracking error. The beamspace method is also extended and applied in conjunction with the wideband Capon method in order to further enhance the DOA estimation resolution. The developed wideband methods are then benchmarked against the wideband Capon algorithms in<sup>8</sup> on real acoustic signature data sets. The test results on several calibrated acoustic signature data sets that contain multiple groups of light or heavy, wheeled or tracked vehicles are presented. These results demonstrate that among all the methods considered here, the wideband geometric mean and its beamspace version provide better overall performance in terms of accuracy of DOA estimation and ability to resolve the individual sources within a formation.

The organization of this paper is as follows. Section 2 describes the wideband DOA estimation problem and reviews the wideband Capon algorithms,<sup>8</sup> namely, the geometric averaging method for combining power spectra at different narrowband frequencies. Section 3 presents the wideband extension of the robust Capon beamforming method to account for the array mismatching problems. In Section 4, the extension of beamspace method to wideband sources is considered. An analytical comparison of the beampattern and bearing responses of different wideband DOA estimation methods is given in Section 5. Test results on real multiple target data runs for 5-element wagon-wheel array are presented in Section 6. A performance benchmarking of all the methods is also provided in this section. Finally, Section 7 gives the concluding remarks about the proposed methods and their usefulness for DOA estimation and tracking of acoustic sources in realistic situations.

## 2. WIDEBAND CAPON DOA ESTIMATION

Let us consider an array of  $M$  sensors that receive the wavefield generated by  $d$  wideband sources in the presence of an arbitrary noise wavefield. The array geometry can be arbitrary but known to the processor. The source signal vector  $\mathbf{s}(t) = [s_1(t), s_2(t), \dots, s_d(t)]^T$  is assumed to be zero mean and stationary over the observation interval  $T_0$ . The source spectral density matrix is denoted by  $\mathbf{P}_s(f)$ ,  $f \in [f_c - BW/2, f_c + BW/2]$  with the bandwidth  $BW$  comparable to the center frequency  $f_c$ . The spectral density matrix  $\mathbf{P}_s(f)$  is a  $d \times d$  nonnegative Hermitian matrix, unknown to the processor. The noise wavefield is assumed to be independent of the source signals with  $M \times M$  noise spectral density matrix  $\mathbf{P}_n(f)$ . Then, the spectral density matrix of the  $M$ -dimensional array output  $\mathbf{x}(t)$  may be written as

$$\mathbf{P}_x(f) = \mathbf{A}(f, \underline{\theta})\mathbf{P}_s(f)\mathbf{A}^H(f, \underline{\theta}) + \mathbf{P}_n(f) \quad (1)$$

where  $\mathbf{A}(f, \underline{\theta}) = [\mathbf{a}(f, \theta_1), \mathbf{a}(f, \theta_2), \dots, \mathbf{a}(f, \theta_d)]$  is the  $M \times d$  array manifold matrix of the sensor array system, with respect to some chosen reference point,  $\mathbf{a}(f, \theta_i)$  is the steering vector of the  $i$ th source, and  $\underline{\theta} = [\theta_1, \dots, \theta_d]$

is the bearing angle vector of the sources. It is assumed that  $M > d$  and that the rank of  $\mathbf{A}(f, \underline{\theta})$  is equal to  $d$  at any frequency and angle of arrival.

The array output vector  $\mathbf{x}(t)$  is first decomposed into narrowband components by taking DFT over non-overlapping time segments of length  $\Delta T$ . That is, the array output  $\mathbf{x}(t)$ , observed over  $T_0$  seconds, is sectioned into  $K$  windows of duration  $\Delta T$  seconds each. Thus,  $\Delta T$  is the duration of one snapshot in the usual terminology of narrowband array processing and  $K$  is the total number of snapshots. We denote the  $j$ th narrowband component of all the DFT outputs of  $K$  snapshots by vector  $\mathbf{x}_k(f_j)$ ,  $k = 1, 2, \dots, K$ , and  $j = 1, 2, \dots, J$ . It is also assumed that the decomposed narrowband components are mutually independent. The goal is to determine the number of sources  $d$  and estimate the angles  $\theta_i$ ,  $i = 1, 2, \dots, d$  from the data  $\mathbf{x}_k(f_j)$ ,  $k = 1, 2, \dots, K$ ;  $j = 1, 2, \dots, J$ . The spatial covariance matrix of the recorded data for the  $j$ th narrowband component  $\mathbf{x}_k(f_j)$  is

$$\mathbf{R}_{\mathbf{xx}}(f_j) \approx \mathbf{P}_{\mathbf{x}}(f_j) = \mathbf{A}(f_j, \underline{\theta})\mathbf{P}_{\mathbf{s}}(f_j)\mathbf{A}^H(f_j, \underline{\theta}) + \mathbf{P}_{\mathbf{n}}(f_j), \quad j = 1, 2, \dots, J. \quad (2)$$

where  $\Delta T$  is assumed to be  $\Delta T = 1$ .

In<sup>8</sup>, several wideband Capon DOA estimation methods were developed that use different spectral averaging schemes to estimate  $\theta_i$ 's using the spatial covariance matrix of the data at narrowband frequencies  $f_j$ . At frequency bin  $f_j$ , the rank-1 narrowband Capon beamformer  $\mathbf{c}(f_j, \theta)$  is defined as the vector that maximizes the signal-to-noise/interference at the output of the beamformer,  $\mathbf{z}_k(f_j) = \mathbf{c}^H(f_j, \theta)\mathbf{x}_k(f_j)$ , for the scalar look-direction angle,  $\theta$ . This problem can be posed<sup>5</sup> by

$$\min_{\mathbf{c}(f_j, \theta)} Q(f_j, \theta) = \mathbf{c}^H(f_j, \theta)\mathbf{R}_{\mathbf{xx}}(f_j)\mathbf{c}(f_j, \theta) \quad (3)$$

under the constraint that  $\mathbf{c}^H(f_j, \theta)\mathbf{a}(f_j, \theta) = 1$ . Note  $\mathbf{R}_{\mathbf{xx}}(f_j) = \sum_{k=1}^K \mathbf{x}_k(f_j)\mathbf{x}_k^H(f_j)$  is the sample covariance matrix and it is assumed that  $\mathbf{c}(f_j, \theta)$  is independent of  $k$  within one snapshot. The solution of this minimization problem leads to the narrowband rank-1 Capon beamformer<sup>5</sup> for  $\mathbf{c}(f_j, \theta) = \frac{\mathbf{R}_{\mathbf{xx}}^{-1}(f_j)\mathbf{a}(f_j, \theta)}{\mathbf{a}^H(f_j, \theta)\mathbf{R}_{\mathbf{xx}}^{-1}(f_j)\mathbf{a}(f_j, \theta)}$  and the Capon spectrum,  $q(f_j, \theta)$ , as

$$q(f_j, \theta) = \frac{1}{\mathbf{a}^H(f_j, \theta)\mathbf{R}_{\mathbf{xx}}^{-1}(f_j)\mathbf{a}(f_j, \theta)} \quad (4)$$

The DOA's are then estimated by searching for the peaks of the Capon spectrum  $q(f_j, \theta)$  for different  $\theta$ .

For the wideband case, however, where all frequency components should be taken into account, the power at the output of the narrowband Capon beamformers, i.e.  $q(f_j, \theta)$ , may be incoherently averaged for all (or a subset) of the narrowband frequencies  $f_j$ ,  $j = 1, \dots, J$ . Results in<sup>8</sup> indicated that among the three averaging methods, namely arithmetic, geometric and harmonic, the geometric averaging gave more accurate DOA estimation. For the geometric wideband Capon, the average output power  $Q_G(\theta)$  is given by

$$Q_G(\theta) = \prod_{j=1}^J q(f_j, \theta) = \prod_{j=1}^J \frac{1}{\mathbf{a}^H(f_j, \theta)\mathbf{R}_{\mathbf{xx}}^{-1}(f_j)\mathbf{a}(f_j, \theta)} \quad (5)$$

The DOAs' may then be estimated by finding the locations of the peaks of  $Q_G(\theta)$ .

### 3. WIDEBAND ROBUST CAPON METHOD

The main problem with the Capon beamformer is that it is not robust against mismatches between the presumed (or theoretical) and actual steering vectors. These mismatches could be caused by sensor location uncertainties, wavefront perturbations and near-field effects. Several approaches have been proposed over the past few years to solve this problem. The robust Capon beamforming method,<sup>10</sup> which belongs to the diagonal loading class of approaches, is based upon an ellipsoidal uncertainty constraint for the steering vector. This method provides an adaptive and more accurate scheme for quantifying the diagonal loading as well as a simpler way for eliminating the scaling ambiguity. In addition to its good interference cancellation property and robustness to small mismatches in the signal models, it maintains a dynamic main-lobe width for receiving the desired signal.

It has been shown<sup>10</sup> that the robust Capon beamformer with ellipsoidal uncertainty constraint is equivalent to solving the following optimization problem under spherical constraint, i.e.

$$\min_{\mathbf{a}} \mathbf{a}^H(f_j, \theta) \mathbf{R}_{\mathbf{xx}}^{-1}(f_j) \mathbf{a}(f_j, \theta) \quad \text{subject to} \quad \|\mathbf{a} - \bar{\mathbf{a}}\|^2 \leq \epsilon \quad (6)$$

where  $\bar{\mathbf{a}}(f_j, \theta)$  is the presumed (normalized) steering vector and  $\epsilon$  is the maximum scalar error constraint. That is, the true steering vector is close to the presumed steering vector within a spherical region with radius  $\epsilon$ . The result of the constrained minimization problem leads to a computationally efficient robust Capon beamformer with the optimal diagonally loaded covariance matrix. This algorithm requires a 1-D search to find the optimum diagonal loading coefficient at each look direction. The steps for the wideband extension of this algorithm are:

1. Compute the Singular Value Decomposition (SVD) of the sample covariance matrix  $\mathbf{R}_{\mathbf{xx}}(f_j)$  as

$$\mathbf{R}_{\mathbf{xx}}(f_j) = \mathbf{E}(f_j) \Lambda(f_j) \mathbf{E}^H(f_j) \quad (7)$$

where  $\Lambda(f_j) = \text{Diag}[\lambda_1, \dots, \lambda_M]$ , with  $\lambda_1 > \lambda_2 > \dots > \lambda_{d+1}$  and  $\lambda_{d+1} = \lambda_{d+2} = \dots = \lambda_M$ , and  $\mathbf{E}(f_j) \in \mathbb{C}^{M \times M}$  contains the signal and noise subspaces, respectively.

2. Solve for the minimizer of

$$g(\gamma_j) = \sum_{m=1}^M \frac{|z_m(f_j)|^2}{(1 + \gamma_j \lambda_m)^2} - \epsilon \quad (8)$$

using a 1-D search (e.g. Newton's method) and get  $g(\gamma_j)$  as close to  $\epsilon$  as possible;  $\gamma_j$  is the optimal diagonal loading factor for frequency  $f_j$  and angle  $\theta$ ;  $z_m(f_j)$  is the  $m^{\text{th}}$  element of  $\mathbf{z}(f_j) = \mathbf{E}^H(f_j) \check{\mathbf{a}}(f_j, \theta)$ , where  $\check{\mathbf{a}}(f_j, \theta)$  is the unnormalized steering vector for the specific frequency and angle, i.e.,  $\check{\mathbf{a}}(f_j, \theta) = \sqrt{M} \cdot \bar{\mathbf{a}}(f_j, \theta)$ .

3. Using (5) compute the geometrically averaged output power by replacing the assumed steering vector  $\bar{\mathbf{a}}(f_j, \theta)$  with

$$\check{\mathbf{a}}(f_j, \theta) = \bar{\mathbf{a}}(f_j, \theta) - \mathbf{E}(f_j) (\mathbf{I} + \gamma_j \Lambda(f_j))^{-1} \mathbf{E}^H(f_j) \bar{\mathbf{a}}(f_j, \theta) \quad (9)$$

which yields the following geometrically averaged robust Capon

$$Q_{G_{Robust}}(\theta) = \prod_{j=1}^J \frac{1}{\bar{\mathbf{a}}^H(f_j, \theta) \mathbf{E}(f_j) \Lambda(f_j) [\gamma_j^{-2} \mathbf{I} + 2\gamma_j^{-1} \Lambda(f_j) + \Lambda^2(f_j)]^{-1} \mathbf{E}^H(f_j) \bar{\mathbf{a}}(f_j, \theta)} \quad (10)$$

When utilizing this algorithm, it is important to take into consideration the added computational demand that is required. Two additional computations other than those in the standard Capon algorithm must be performed: the SVD of the Hermitian matrix  $\mathbf{R}_{\mathbf{xx}}$ , (computational demand of  $O(M^3)$  flops) and the 1-D search method to find the optimal loading factor. However, it should be noted that it is not necessary to perform the inverse of  $\mathbf{R}_{xx}$  (computation demand of  $O(M^3)$ ), and hence the computational complexity for the robust Capon is close to that of the standard Capon algorithm.

#### 4. WIDEBAND BEAMSPACE CAPON METHOD

The beamspace method reduces the complexity and degrees of freedom in an array by steering a group of *beams* instead of the phasings of the individual sensors. The  $M \times M_{bs}$  beamspace matrix  $B_{bs}$  is a projection matrix from the element space (size  $\mathbb{C}^M$ ) to the beamspace (size  $\mathbb{C}^{M_{bs}}$ ) ( $M \geq M_{bs}$ ). Finding covariance with respect to these beams instead of the elements focuses the region of interest (or region of active interference cancellation) and dramatically attenuates signals outside this region. This yields better beamformed data as a result of the focusing of the algorithm on a particular region of interest. This also reduces the amount of processing as the size of the covariance matrix reduces from  $M \times M$  to  $M_{bs} \times M_{bs}$ . This could be especially important in medium to large distributed sensor networks.

The principle idea behind beamspace is based upon the assumption that the signal of interest is not taking up the entire element signal space and is in a smaller dimension subspace. This can however produce ambiguities.<sup>11</sup> Beamspace pre-processing projects the input data vector into a subspace where the signal of interest will be extracted easier, while canceling signals outside the filtering region of interest. Hence, the algorithm acts as a spatial bandpass filter.

In the reduced-dimension beamspace, the outputs of the  $M$ -element standard array are processed to produce  $M_{bs}$  orthogonal beams. The center beam is a conventional beam pointed at the look direction, which is called the **Main Response Axis** (MRA). It is important that the beams be orthogonal, this ensures that any signal arriving along the main lobe of a particular beam will not produce output from any other beam. The  $M \times M_{bs}$  matrix  $B_{bs}$ , ( $M_{bs} = M$  for full-dim BS), is formed with the steering vectors of each beam. This set is called the beamfan. To implement the beamspace method, a beamfan is formed of  $M_{bs}$  beams and the MRA is steered to the look direction. The beamfan is moved through all electrical angles to obtain the power spectrum. A general form of a non-orthogonalized beamspace matrix is

$$B_{no}(f_j, \theta) = [ \mathbf{b}(f_j, \phi_{-P} + \theta) \quad \dots \quad \mathbf{b}(f_j, \phi_0 + \theta) \quad \dots \quad \mathbf{b}(f_j, \phi_P + \theta) ] \quad (11)$$

where

$$\mathbf{b}(f_j, \tau) = \begin{bmatrix} e^{j2\pi f_j/c(\alpha_0 \cos(\tau) + \beta_0 \sin(\tau))} \\ e^{j2\pi f_j/c(\alpha_1 \cos(\tau) + \beta_1 \sin(\tau))} \\ \vdots \\ e^{j2\pi f_j/c(\alpha_{M-1} \cos(\tau) + \beta_{M-1} \sin(\tau))} \end{bmatrix}, \quad (12)$$

and  $\phi_{-P}, \dots, \phi_0, \dots, \phi_P$  are the angles of each of the beams ( $\mathbf{b}(f_j, \tau)$ ) in the beamspace matrix,  $c$  is the speed of sound in air,  $\alpha_i$  and  $\beta_i$  are the horizontal and vertical positions of the  $i^{th}$  sensor relative to the reference position. In the case of the wagon-wheel circular array,  $\alpha_i = \beta_i = r$  (except for the reference element at  $\alpha_0 = \beta_0 = 0$ ), where  $r$  is the radius of the array. To ensure orthogonality of the beamspace matrix, we compute

$$B_{bs} = B_{no}[B_{no}^H B_{no}]^{-\frac{1}{2}} \quad (13)$$

Clearly orthogonality results in  $B_{bs}^H B_{bs} = \mathbf{I}_{M_{bs}}$ . The received data is then preprocessed using the beamspace matrix  $B_{bs}$  prior to any beamforming process. The processing steps in the wideband beamspace method are listed below.

1. Transform the array output vector,  $\mathbf{x}_k(f_j)$ ,  $k = 1, 2, \dots, K$  using

$$\mathbf{v}_k(f_j) = B_{bs}^H(f_j, \theta) \mathbf{x}_k(f_j) \quad (14)$$

where  $B_{bs}(f_j, \theta)$  is the  $M \times M_{bs}$  beamspace matrix whose columns are the orthogonal beampatterns (or other optimized beams) centered around  $\theta$  and frequency  $f_j$ . The resulting sample covariance matrix of the transformed array output,  $\mathbf{v}_k(f_j)$  is

$$\begin{aligned} R_{\mathbf{v}\mathbf{v}}(f_j) &= B_{bs}^H(f_j, \theta) R_{\mathbf{x}\mathbf{x}}(f_j) B_{bs}(f_j, \theta) \\ &\approx B_{bs}^H(f_j, \theta) A(f_j, \theta) \mathbf{P}_{\mathbf{s}}(f_j) A^H(f_j, \theta) B_{bs}(f_j, \theta) + B_{bs}^H(f_j, \theta) \mathbf{P}_{\mathbf{n}}(f_j) B_{bs}(f_j, \theta) \end{aligned} \quad (15)$$

where  $A(f_j, \theta)$ ,  $\mathbf{P}_{\mathbf{s}}(f_j)$ , and  $\mathbf{P}_{\mathbf{n}}(f_j)$  were defined before.

2. The transformed steering vector is given as

$$\mathbf{a}_{bs}(f_j, \theta) = B_{bs}^H(f_j, \theta) \mathbf{a}(f_j, \theta) \quad (16)$$

and the beamformer output becomes  $\mathbf{z}_k(f_j, \theta) = \mathbf{c}_{bs}^H(f_j, \theta) \mathbf{v}_k(f_j)$ , where

$$\mathbf{c}_{bs}(f_j, \theta) = \frac{R_{\mathbf{v}\mathbf{v}}^{-1}(f_j) \mathbf{a}_{bs}(f_j, \theta)}{\mathbf{a}_{bs}^H(f_j, \theta) R_{\mathbf{v}\mathbf{v}}^{-1}(f_j) \mathbf{a}_{bs}(f_j, \theta)}. \quad (17)$$

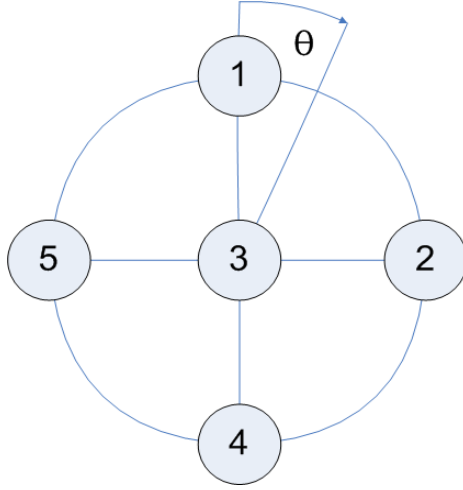


**Figure 1.** 5-element wagon wheel circular array and numbering of its elements.

3. The wideband geometric mean beamspace power spectrum output then becomes

$$Q_{G_{bs}}(\theta) = \prod_{j=1}^J \frac{1}{\mathbf{a}_{bs}^H(f_j, \theta) \mathbf{R}_{\mathbf{v}\mathbf{v}}^{-1}(f_j) \mathbf{a}_{bs}(f_j, \theta)}. \quad (18)$$

The beamspace preprocessing method requires some additional computations when compared to the wideband geometric Capon. This is mostly due to the whitening process for the beamspace matrix at each look direction and frequency bin. However, in more general applications of beamspace, especially those involving large numbers of sensors, the beamspace algorithm actually decreases the computational complexity. Beamspace is also very effective when the normalized average period ( $K/M$ ) is small. The algorithm allows the statistical convergence of the covariance matrix to steady state because of its reduced size. The algorithm can form these statistically stable covariance matrices with a fraction of the observations required by normal dimension algorithms.<sup>5</sup>

## 5. ANALYSIS OF DIFFERENT WIDEBAND DOA ESTIMATION METHODS

Next, we study the 2D output power of the wideband geometric Capon, the wideband robust Capon and the wideband beamspace algorithms with respect to the true angle and the look angle. Let us denote the look angle by  $\theta$  and the true angle of a single source by  $\phi$ . The steering vector for the 5-element wagon-wheel array is  $\mathbf{a}(f_j, \theta) = [e^{-j2\pi f_j r / c \cos \theta} \ e^{-j2\pi f_j r / c \sin \theta} \ 1 \ e^{j2\pi f_j r / c \cos \theta} \ e^{j2\pi f_j r / c \sin \theta}]^T$ . Note that here  $f_j$  is the  $j^{th}$  narrowband frequency,  $r$  is the radius of the array (in this case .6096 m), and  $c$  is the speed of sound in air (335 m/s). The wagon-wheel array elements are numbered as: North-element 1, East-element 2, Center (reference)-element 3, South-element 4, and West-element 5, as shown in Figure 1.

For a narrowband source of frequency  $f_j$  at angle  $\phi$  the received signal vector for the wagon-wheel array can also be represented by,

$$\mathbf{x}(f_j) = [e^{-j2\pi f_j r / c \cos \phi} \ e^{-j2\pi f_j r / c \sin \phi} \ 1 \ e^{j2\pi f_j r / c \cos \phi} \ e^{j2\pi f_j r / c \sin \phi}]^T. \quad (19)$$

For the noise-free case, the rank-1 covariance matrix of the received signal is  $\mathbf{R}_{\mathbf{xx}} = \mathbf{xx}^H$ . Diagonal loading of the covariance matrix was used to avoid singularity problems and to simulate noise effects.

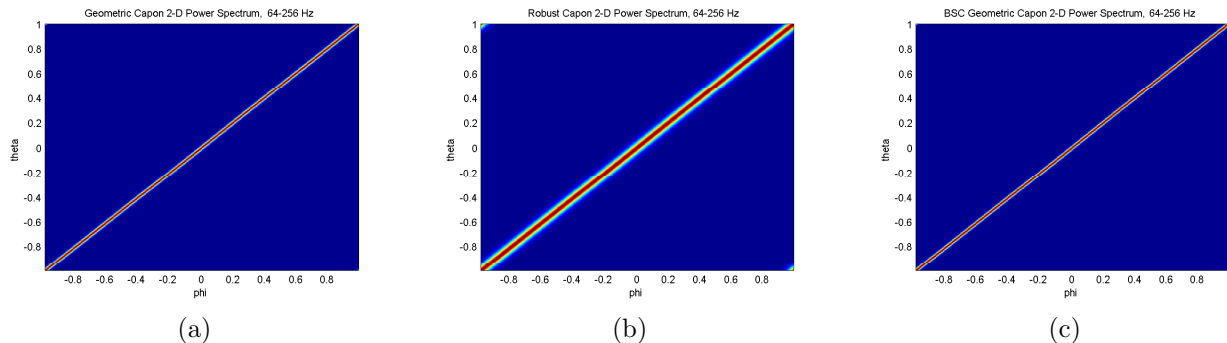


**Figure 2.** Power spectrums for (a) Geometric mean Capon, (b) Geometric mean robust Capon (with error,  $\epsilon = .7$ ), (c) Geometric mean Beamspace Capon with respect to look direction ( $\theta$ ) and angle of arrival ( $\phi$ ).

The synthesized data was then generated using the above source model. A set of narrowband frequencies with 16 Hz separation and equal power were used in the frequency range of 64 to 256 Hz (typical for vehicles). The reason for not considering frequencies higher than 256Hz is that the aliasing frequency for the wagon-wheel array is approximately 277Hz.<sup>8</sup> In the 2-D power spectrum synthesis the beamspace Capon algorithm used 3 beams at  $-6^\circ$ ,  $0^\circ$ , and  $6^\circ$ , and an estimated error of 1.5 was used for the robust Capon method. Figures 2(a)-(c) show the 2D output power for the geometric mean, robust Capon, and beamspace Capon, respectively. These correspond to the plots of  $Q_G$  (geometric),  $Q_{GRC}$  (robust Capon), and  $Q_{G_{bs}}$  (beamspace Capon) with respect to true angle  $\theta$  and look angle  $\phi$ . The geometric mean Capon, as shown in Figure 2(a), exhibits a narrow main-lobe without noticeable side-lobe structure. This is due to the fact that the geometric mean is based upon the product operation where the lower frequencies eliminate any side-lobes, while the higher frequencies narrow the beamwidth and hence giving better overall resolution. This may also eliminate any low-power sources located further away, as it is very difficult to distinguish between side-lobes and far away targets. The robust Capon, on the other hand, has a wider beamwidth than the standard geometric Capon. The beamwidth is wider because of the initial estimate of the steering vector error ( $\epsilon$ ) that the algorithm used to find the optimal diagonal loading factor, i.e. the optimal beamwidth for beamforming to a signal or array mismatch, without losing the cancelation properties of the Capon algorithm. The geometrically averaged beamspace Capon also exhibits a narrow main-lobe because of the improved resolution of the beamspace method. Although the improvement of beamspace over the standard geometric averaging is not noticeable in the 2-D beampattern, the algorithm does indeed act as a spatial filter for noise and other interference. This advantage will be shown more prominently on real data (see the next section), especially when multiple closely spaced sources must be detected in presence of wind noise.

Both the beamspace and robust Capon have similar performance in different model mismatch situations. Two narrowband experiments were conducted to investigate the robustness of these methods. In the first experiment the array elements were perturbed in location by a Gaussian random variable with zero mean and variance 1 ( $\sigma = 1$ ). This results in beampattern sidelobes that are higher but the mainlobe still adequately matches to the source angle. In the second experiment a displacement of  $\delta\theta = 4^\circ$  of the source from the true direction was introduced. Here, both the beamspace and robust Capon algorithms were able to match similarly to the source. The results of these experiments are illustrated in the 1-D power spectra shown in Figures 3(a)-(b) for the beamspace algorithm with beams at  $-10^\circ$ ,  $-5^\circ$ ,  $0^\circ$ ,  $5^\circ$ , and  $10^\circ$ , and the robust Capon having estimated error of 1, respectively.

## 6. DOA ESTIMATION RESULTS

In this section, the wideband DOA estimation algorithms detailed in this paper are applied to the calibrated data of two multiple target runs in the acoustic signature database. The wideband robust Capon beamformer in section 3 is applied to uncalibrated data to show advantages over basic geometrically averaged Capon. In these runs, the wideband beamspace Capon is implemented with 3 beams at  $-6^\circ$ ,  $0^\circ$ , and  $6^\circ$  from the look direction.

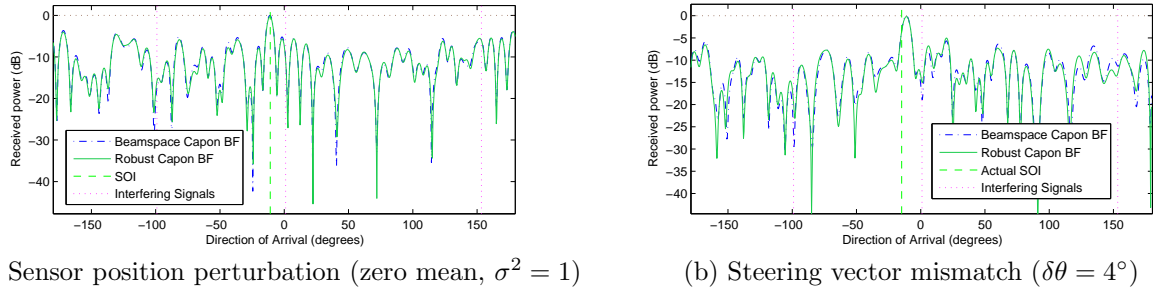


**Figure 3.** Narrowband beampatterns for the standard, robust, and beamspace Capon algorithms illustrating robustness to perturbations.

The data calibration process accounts for the errors caused by differences between the presumed values of array parameters, namely gain, phase, and sensor positions, and the values of these parameters after the array was deployed. Prior to DOA estimation, the time series recorded by each microphone is first filtered using a sliding Hamming window of size 2048 (corresponding to 2 seconds of data) with 50% overlap. The calibration is then performed on each 2048 samples for the frequency range of 50-250Hz. Since the sampling frequency for the collected data set is 1024Hz and the size of the sliding Hamming window is 2048, the resultant calibrated data has twice the length of the uncalibrated data. Therefore, in the DOA estimation, a time window of size 2048 samples will be considered as one snapshot. In order to report a DOA estimate every second, a 50% overlap is considered between the time windows.

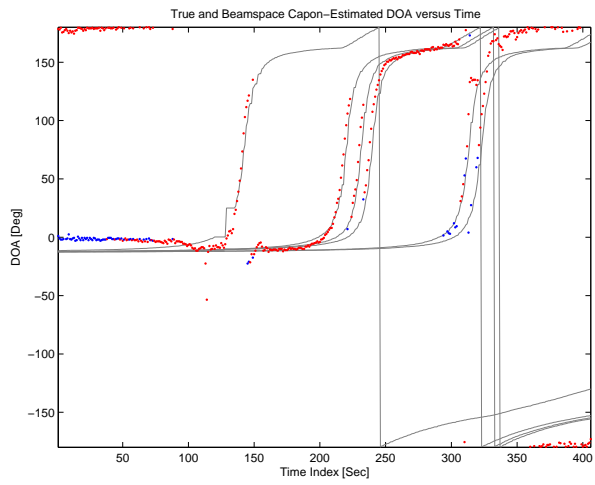
### 6.1. Results on Run 1

This run contains six targets that move in three separate groups. The first group contains a single light wheeled vehicle, the second group is formed of three heavy tracked vehicles, and the third group includes two heavy wheeled vehicles. Figures 4(a)-(b) show the DOA estimation results on the calibrated data of Run 1 obtained using the beamspace Capon and the original geometric Capon algorithms, respectively. Solid lines correspond to the actual (true) angles obtained from the truth file. Comparison of the methods clearly showed improved tracking and decreased variability in the estimated DOA's for the beamspace approach. This is because the beamspace algorithm works with a reduced data set of spectral information to beamform with. Thus, interference cancelation occurs only on the spectral data near the look direction. The improvements of the beamspace Capon become even more prominent when there are fewer frequency bins to average over, or when the number of samples used to create the covariance matrix are limited. In these cases, the beamspace Capon maintained better DOA estimates and lower variability due to its inherent robustness to a low number of samples. This property of the beamspace method is a direct consequence of the reduced dimension. That is, the ratio of samples to processing elements (beams or sensors) stays much higher, hence making better sample data for beamforming from which to calculate DOA's.

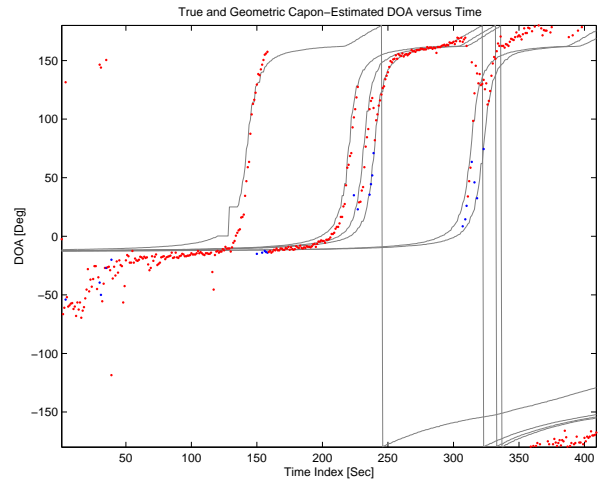
The uncalibrated data of Run 1 was used to examine the real usefulness of the robust wideband Capon when there are uncertainties in the locations (phase error) and gains of the microphones. The value of the assumed steering vector error was chosen to be  $\epsilon = .7$ . The DOA estimation results of the wideband robust Capon are shown in Figure 5(a). Clearly, when compared with the results of the original geometric wideband Capon in Figure 4(b), which is obtained using the calibrated data, there appears to be no real advantage for using the robust Capon method. However, if the original geometric Capon is applied to the uncalibrated data (see Figure 5(b)) it is evident that the robust geometric Capon provides more accurate DOA estimates, especially when the targets are in the near-field ( $T = 160...320$ ). This is attributed to the fact that at near-field, the robust Capon not only accounts for the array mismatches due to the sensor location errors but also those of near-field effects.

### 6.2. Results on Run 2

This run contains four moving and two stationary targets. These are: four light wheeled, and two light tracked vehicles. Unfortunately, the information as to which track corresponds to which target was not available. This

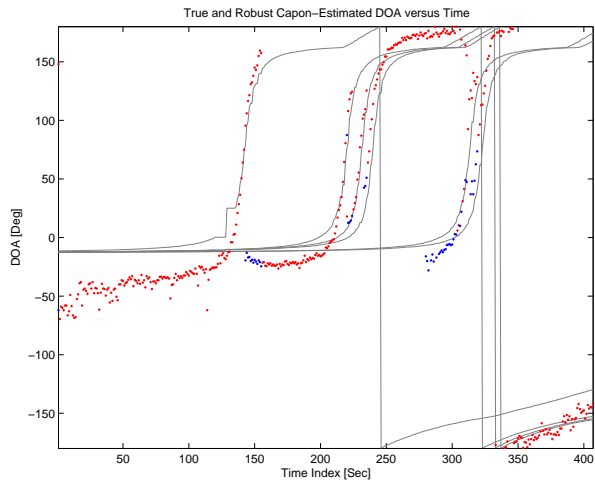


(a) Beamspace Capon

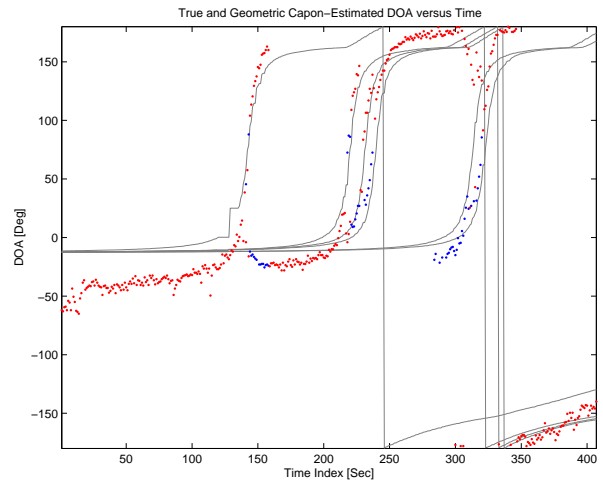


(b) Geometric Capon

**Figure 4.** DOA Estimates of Wideband Beamspace Capon and original Wideband Geometric Mean Capon Algorithms - Calibrated data of Run 1.



(a) Robust Capon



(b) Geometric Capon

**Figure 5.** DOA Estimates of wideband Robust Capon ( $\epsilon = .7$ ) and original Wideband Geometric Mean Capon algorithms - Uncalibrated data of Run 1.

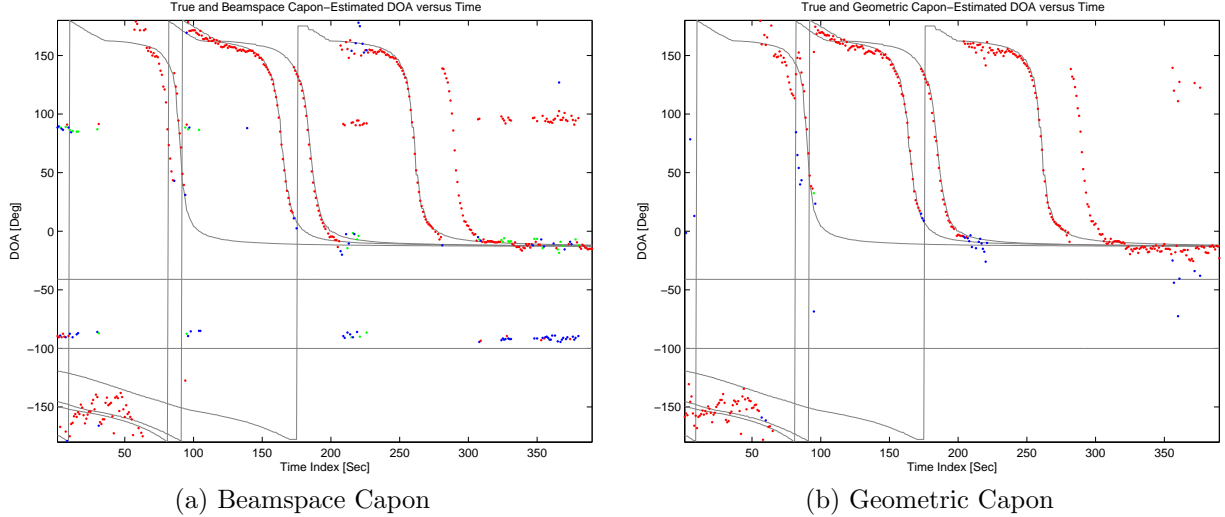


**Figure 6.** DOA Estimates of Wideband Beamspace Capon and original Wideband Geometric Mean Capon Algorithms - Calibrated data of Run 2.

particular run was chosen to determine the effectiveness of the developed algorithms in adverse environmental conditions where the wind noise is very high.

Figures 6(a)-(b) show the DOA estimation results, obtained using the wideband beamspace Capon and geometric Capon algorithms, respectively. As can be seen, all the tracks are successfully detected in both methods. The beamspace algorithm tracked all the targets well. The improvements were more evident especially near the end of the run, where the DOA estimates are more consistent. However, a pitfall of using the beamspace method with the circular array geometry specified above is that in low SNR situations, DOA ambiguities can appear along the symmetry axes of an array. For this array, these ambiguities are at  $\pm 90^\circ$ ,  $0$ , and  $\pm 180^\circ$ . Finally, what is strange for this run is that all the methods detected an extra track which was not in the truth file. We note that the stationary targets cannot be detected as they are very far (approximately 4 and 8 km) from the nodes.

Figures 7(a)-(b) show the DOA estimation results on uncalibrated data for Run 2 using the wideband robust and geometric Capon beamformers, respectively. Similar observations can be made for this run. That is, near-field targets are resolved somewhat better with the robust Capon beamformer, although the improvement is not dramatic and the robust Capon does have some spurious estimates.

### 6.3. Results on a Single Target Run 3 - Accuracy Analysis

To further benchmark the original wideband geometric mean Capon with its beamspace version in Section 4 in terms of DOA accuracy a single target run was used in this experiment. This particular run contains a heavy wheeled vehicle. The DOA estimates at all snapshots generated using these two methods were compared against the true DOA's. Figures 8(a)-(b) show the DOA estimation results of these two methods on this single-target run. Figures 8(c) and (d) show the distribution of the DOA error for the wideband beamspace and original geometric Capon methods, respectively. The mean errors are  $4.477^\circ$  and  $4.50^\circ$  for the wideband beamspace Capon and wideband geometric Capon, respectively. The variance of the errors are  $4^\circ$  and  $5.5^\circ$  for the wideband beamspace Capon and wideband geometric Capon, respectively. The lower variance for the beamspace is an indication of a slightly better tracking performance. As is evident, filtering out spatial noise with the beamspace algorithm has the effect of reducing tracking error and improving resolution.

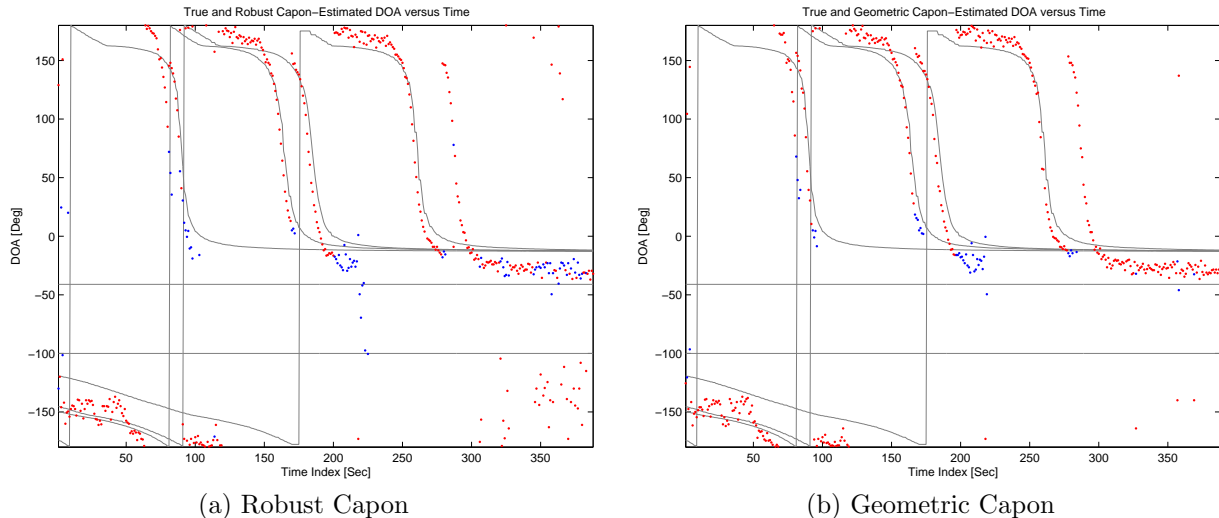


**Figure 7.** DOA Estimates of wideband Robust Capon ( $\epsilon = .7$ ) and original Wideband Geometric Mean Capon algorithms - Uncalibrated data of Run 2.

## 7. OBSERVATIONS & CONCLUSIONS

This paper presents improvements on wideband DOA estimation methods for separating and tracking multiple acoustic sources, namely ground vehicles, in the presence of array perturbations and model mismatches. A robust Capon beamforming algorithm was extended to the wideband case to attempt to account for the array steering vector mismatches caused by sensor location error and wavefront perturbations. To improve the resolution and robustness to limited observation vectors or high noise, the beamspace method was also extended to wideband. A comprehensive study was then carried out to benchmark these methods in terms of their beamwidth, DOA accuracy and robustness in the presence of sensor location error and near-field effects. It was observed that the wideband robust geometric Capon provided better overall results on the uncalibrated data when compared to the original wideband geometric mean Capon. This was more evident in near-field situations. This improvement is obtained without the dramatic increase of the computational complexity. It was shown<sup>10</sup> previously that the computational complexity of the robust Capon beamforming method is comparable to that of the standard Capon beamformer. Although, the beamspace method did not provide substantially better results on multiple-target cases, the mean and variance of DOA tracking error was reduced when compared with the original geometric mean Capon. The beamspace Capon also provided better results when less than an adequate number of observations were available for constructing the covariance matrix. The results on Run 1 also indicated better performance of the beamspace method at farther range when the detection of targets becomes more difficult. Also, when wind effects were high (in Run 2) this algorithm provided very good results due to its spatial filtering property.

## ACKNOWLEDGMENTS

This work is funded by Army SBIR-Phase II contract # DAAE30-03-C-1055. The data and technical support has been provided by the US Army TACOM-ARDEC, Picatinny Arsenal, NJ. The authors would like to thank Mr. Bob Wade at U.S. Army Picatinny Arsenal for his suggestions and technical support.

## REFERENCES

1. N. Srour, "Unattended ground sensors - a prospective for operational needs and requirements," tech. rep., ARL Report Prepared for NATO, October, 1999.
2. T. Pham and M. Fong, "Real-time implementation of MUSIC for wideband acoustic detection and tracking," *Proc. of SPIE AeroSense'97: Automatic Target Recognition VII*, (Orlando, FL), April, 1997.

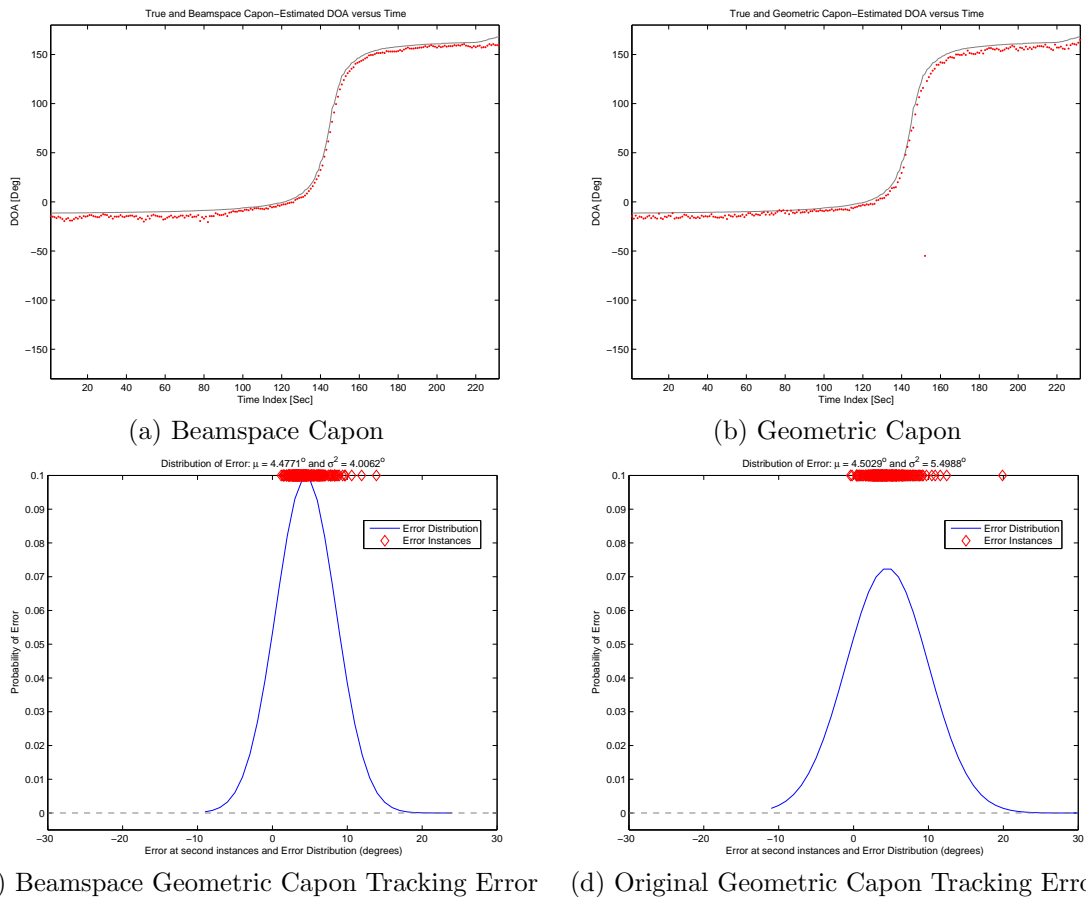


**Figure 8.** DOA estimates and DOA Error Distributions on a single target run. Distributions result in means of  $4.47^\circ$  and  $4.5^\circ$  and variances  $4^\circ$  and  $5.5^\circ$  for the beamspace and original geometric mean Capon beamformers, respectively.

3. T. Pham and B. M. Sadler, "Wideband array processing algorithms for acoustic tracking of ground vehicles," tech. rep., Army Research Laboratories, Adelphi, MD, 1997.
4. J. Krolik, *Advances in Spectrum Analysis and Array Processing, Vol. II*, ch. 6: Focused wideband array processing for spatial spectral estimation. Prentice-Hall, 1991.
5. H. L. VanTrees, *Optimum Array Processing*, Wiley Interscience, 2002.
6. E. D. D. Claudio and R. Parisi, "WAVES: Weighted Average of Signal subspaces for robust wideband direction finding," *IEEE Transactions on Signal Processing*, vol. 49, pp. 2179 – 2191, 2001.
7. H. Wang and M. Kaveh, "Coherent signal-subspace processing for the detection and estimation of angles of arrival of multiple wide-band sources," *IEEE Transactions on Acoustics, Speech, and Signal Processing*, vol. 33, pp. 823 – 831, 1985.
8. M. R. Azimi-Sadjadi, A. Pezeshki, L. Scharf, and M. Hohil, "Wideband DOA estimation algorithms for multiple target detection and tracking using unattended acoustic sensors," *Proc. of SPIE-Defense and Security*, vol. 5417, pp. 1–11, (Orlando, FL), April 2004.
9. H. Hung and M. Kaveh, "Focussing matrices for coherent signal-subspace processing," *IEEE Transactions on Acoustics, Speech, and Signal Processing*, vol. 36, pp. 1272 – 1281, 1988.
10. J. Li, P. Stoica, and Z. Wang, "On robust Capon beamforming and diagonal loading," *IEEE Trans. on Signal Processing*, vol. 51, pp. 1702–1715, 2003.
11. A. Amini and T. Georgiou, "Avoiding ambiguity in beamspace processing," *IEEE Signal Processing Letters*, vol. 12 Issue 5, pp. 372 – 375, 2005.